Biomedical Optics EXPRESS

Imaging and full-length biometry of the eye during accommodation using spectral domain OCT with an optical switch

Marco Ruggeri,[1,2,*] Stephen R. Uhlhorn,[1] Carolina De Freitas,[1] Arthur Ho,[3,4,5] Fabrice Manns,[1,2] and Jean-Marie Parel[1,2,4]

[1]*Ophthalmic Biophysics Center, Bascom Palmer Eye Institute, University of Miami Miller School of Medicine, 1638 NW 10th Ave. Miami, FL 33136, USA*
[2]*Biomedical Optics and Laser Laboratory, Department of Biomedical Engineering, University of Miami, College of Engineering, Coral Gables, FL,33146 USA*
[3]*Brien Holden Vision Institute, Sydney, NSW, Australia*
[4]*Vision Cooperative Research Centre, Sydney, NSW, Australia*
[5]*School of Optometry & Vision Science, University of New South Wales, Australia*
**mruggeri@med.miami.edu*

Abstract: An optical switch was implemented in the reference arm of an extended depth SD-OCT system to sequentially acquire OCT images at different depths into the eye ranging from the cornea to the retina. A custom-made accommodation module was coupled with the delivery of the OCT system to provide controlled step stimuli of accommodation and disaccommodation that preserve ocular alignment. The changes in the lens shape were imaged and ocular distances were dynamically measured during accommodation and disaccommodation. The system is capable of dynamic *in vivo* imaging of the entire anterior segment and eye-length measurement during accommodation in real-time.

OCIS codes: (170.4500) Optical coherence tomography; (170.3880) Medical and biological imaging; (170.4580) Optical diagnostics for medicine; (330.7322) Visual optics, accommodation; (330.4460) Ophthalmic optics and devices.

References and links

1. C. M. Schor and S. R. Bharadwaj, "A pulse-step model of accommodation dynamics in the aging eye," Vision Res. **45**(10), 1237–1254 (2005).
2. J. A. Mordi and K. J. Ciuffreda, "Dynamic aspects of accommodation: age and presbyopia," Vision Res. **44**(6), 591–601 (2004).
3. A. P. Beers and G. L. Van Der Heijde, "*In vivo* determination of the biomechanical properties of the component elements of the accommodation mechanism," Vision Res. **34**(21), 2897–2905 (1994).
4. S. Kasthurirangan, A. S. Vilupuru, and A. Glasser, "Amplitude dependent accommodative dynamics in humans," Vision Res. **43**(27), 2945–2956 (2003).
5. E. Gambra, Y. Wang, J. Yuan, P. B. Kruger, and S. Marcos, "Dynamic accommodation with simulated targets blurred with high order aberrations," Vision Res. **50**(19), 1922–1927 (2010).
6. G. Heron and W. N. Charman, "Accommodation as a function of age and the linearity of the response dynamics," Vision Res. **44**(27), 3119–3130 (2004).
7. H. A. Anderson, A. Glasser, R. E. Manny, and K. K. Stuebing, "Age-related changes in accommodative dynamics from preschool to adulthood," Invest. Ophthalmol. Vis. Sci. **51**(1), 614–622 (2010).
8. A. P. Beers and G. L. van der Heijde, "Age-related changes in the accommodation mechanism," Optom. Vis. Sci. **73**(4), 235–242 (1996).
9. G. L. van der Heijde, A. P. Beers, and M. Dubbelman, "Microfluctuations of steady-state accommodation measured with ultrasonography," Ophthalmic Physiol. Opt. **16**(3), 216–221 (1996).
10. W. Drexler, A. Baumgartner, O. Findl, C. K. Hitzenberger, and A. F. Fercher, "Biometric investigation of changes in the anterior eye segment during accommodation," Vision Res. **37**(19), 2789–2800 (1997).
11. R. Subramanian, C. Cook, M. Croft, K. L. DePaul, M. Neider, N. J. Ferrier, P. L. Kaufman, and J. F. Koretz, "Unilateral real-time Scheimpflug videography to study accommodation dynamics in human eyes," Invest. Ophthalmol. Vis. Sci. **44**, ARVO E-Abstract 240 (2003).
12. S. R. Uhlhorn, D. Borja, F. Manns, and J. M. Parel, "Refractive index measurement of the isolated crystalline lens using optical coherence tomography," Vision Res. **48**(27), 2732–2738 (2008).

#166403 - $15.00 USD Received 10 Apr 2012; revised 21 May 2012; accepted 1 Jun 2012; published 6 June 2012

13. I. Grulkowski, M. Gora, M. Szkulmowski, I. Gorczynska, D. Szlag, S. Marcos, A. Kowalczyk, and M. Wojtkowski, "Anterior segment imaging with Spectral OCT system using a high-speed CMOS camera," Opt. Express **17**(6), 4842–4858 (2009).
14. J. Jungwirth, B. Baumann, M. Pircher, E. Götzinger, and C. K. Hitzenberger, "Extended *in vivo* anterior eye-segment imaging with full-range complex spectral domain optical coherence tomography," J. Biomed. Opt. **14**(5), 050501 (2009).
15. H. Furukawa, H. Hiro-Oka, N. Satoh, R. Yoshimura, D. Choi, M. Nakanishi, A. Igarashi, H. Ishikawa, K. Ohbayashi, and K. Shimizu, "Full-range imaging of eye accommodation by high-speed long-depth range optical frequency domain imaging," Biomed. Opt. Express **1**(5), 1491–1501 (2010).
16. B. Potsaid, V. Jayaraman, J. G. Fujimoto, J. Jiang, P. J. S. Heim, and A. E. Cable, "MEMS tunable VCSEL light source for ultrahigh speed 60kHz—1MHz axial scan rate and long range centimeter class OCT imaging," Proc. SPIE **8213**, 82130M (2012).
17. C. Dai, C. Zhou, S. Fan, Z. Chen, X. Chai, Q. Ren, and S. Jiao, "Optical coherence tomography for whole eye segment imaging," Opt. Express **20**(6), 6109–6115 (2012).
18. A. Dhalla, T. Bustamante, D. Nanikivil, H. Hendargo, R. McNabb, A. Kuo, and J. A. Izatt, "Dual-depth SSOCT for simultaneous complex resolved anterior segment and conventional retinal imaging," Proc. SPIE **8213**, 82131G (2012).
19. G. Häusler and M. W. Lindner, "'Coherence radar' and 'spectral radar'—new tools for dermatological diagnosis," J. Biomed. Opt. **3**(1), 21–31 (1998).
20. H. Lim, M. Mujat, C. Kerbage, E. C. Lee, Y. Chen, T. C. Chen, and J. F. de Boer, "High-speed imaging of human retina *in vivo* with swept-source optical coherence tomography," Opt. Express **14**(26), 12902–12908 (2006).
21. M. Wojtkowski, R. Leitgeb, A. Kowalczyk, T. Bajraszewski, and A. F. Fercher, "*In vivo* human retinal imaging by Fourier domain optical coherence tomography," J. Biomed. Opt. **7**(3), 457–463 (2002).
22. C. Dorrer, N. Belabas, J. P. Likforman, and M. Joffre, "Spectral resolution and sampling issues in Fourier transform spectral interferometry," J. Opt. Soc. Am. B **17**(10), 1795–1802 (2000).
23. H. Wang, Y. Pan, and A. M. Rollins, "Extending the effective imaging range of Fourier-domain optical coherence tomography using a fiber optic switch," Opt. Lett. **33**(22), 2632–2634 (2008).
24. American National Standards Institute, *Safe Use of Lasers*, ANSI-Z136.1 (ANSI, 1993).
25. D. A. Atchison, A. Bradley, L. N. Thibos, and G. Smith, "Useful variations of the Badal optometer," Optom. Vis. Sci. **72**(4), 279–284 (1995).
26. N. C. Strang, M. Day, L. S. Gray, and D. Seidel, "Accommodation steps, target spatial frequency and refractive error," Ophthalmic Physiol. Opt. **31**(5), 444–455 (2011).
27. F. S. Said and R. A. Weale, "The variation with age of the spectral transmissivity of the living human crystalline lens," Gerontologia **3**(4), 213–231 (1959).
28. S. R. Uhlhorn, F. Manns, H. Tahi, R. O. Pascal, and J. M. Parel, "Corneal group refractive index measurement using low-coherence interferometry," Proc. SPIE **3246**, 14–21 (1998).
29. D. A. Atchison and G. Smith, "Chromatic dispersion of the ocular media of human eyes," J. Opt. Soc. Am. A **22**(1), 29–37 (2005).
30. N. Nassif, B. Cense, B. Hyle Park, S. H. Yun, T. C. Chen, B. E. Bouma, G. J. Tearney, and J. F. de Boer, "*In vivo* human retinal imaging by ultrahigh-speed spectral domain optical coherence tomography," Opt. Lett. **29**(5), 480–482 (2004).
31. M. Dubbelman, G. L. Van der Heijde, and H. A. Weeber, "Change in shape of the aging human crystalline lens with accommodation," Vision Res. **45**(1), 117–132 (2005).
32. J. M. Schmitt, S. L. Lee, and K. M. Yung, "An optical coherence microscope with enhanced resolving power in thick tissue," Opt. Commun. **142**(4-6), 203–207 (1997).
33. F. Lexer, C. K. Hitzenberger, W. Drexler, S. Molebny, H. Sattmann, M. Sticker, and A. F. Fercher, "Dynamic coherent focus OCT with depth independent transversal resolution," J. Mod. Opt. **46**, 541–553 (1999).
34. W. Drexler, U. Morgner, F. X. Kärtner, C. Pitris, S. A. Boppart, X. D. Li, E. P. Ippen, and J. G. Fujimoto, "*In vivo* ultrahigh-resolution optical coherence tomography," Opt. Lett. **24**(17), 1221–1223 (1999).
35. B. Qi, A. P. Himmer, L. M. Gordon, X. D. Yang, L. D. Dickensheets, and I. A. Vitkin, "Dynamic focus control in high-speed optical coherence tomography based on a microelectromechanical mirror," Opt. Commun. **232**(1-6), 123–128 (2004).
36. J. Holmes, S. Hattersley, N. Stone, F. Bazant-Hegemark, and H. Barr, "Multi-channel Fourier domain OCT system with superior lateral resolution for biomedical applications," Proc. SPIE **6847**, 68470O, 68470O-9 (2008).
37. C. Zhou, J. Wang, and S. Jiao, "Dual channel dual focus optical coherence tomography for imaging accommodation of the eye," Opt. Express **17**(11), 8947–8955 (2009).
38. A. G. Bennett, "A method of determining the equivalent powers of the eye and its crystalline lens without resort to phakometry," Ophthalmic Physiol. Opt. **8**(1), 53–59 (1988).
39. M. Dubbelman and G. L. Van der Heijde, "The shape of the aging human lens: curvature, equivalent refractive index and the lens paradox," Vision Res. **41**(14), 1867–1877 (2001).
40. C. P. de Freitas, M. Ruggeri, S. Uhlhorn, F. Manns, and J. M. Parel, "Refractive index of the *in vivo* human crystalline lens measured using whole-eye optical coherence tomography," Invest Ophthalmol Vis Sci **53**, E-Abstract 1341 (2012).

#166403 - $15.00 USD Received 10 Apr 2012; revised 21 May 2012; accepted 1 Jun 2012; published 6 June 2012

41. S. Ortiz, D. Siedlecki, I. Grulkowski, L. Remon, D. Pascual, M. Wojtkowski, and S. Marcos, "Optical distortion correction in optical coherence tomography for quantitative ocular anterior segment by three-dimensional imaging," Opt. Express **18**(3), 2782–2796 (2010).
42. A. Podoleanu, I. Charalambous, L. Plesea, A. Dogariu, and R. Rosen, "Correction of distortions in optical coherence tomography imaging of the eye," Phys. Med. Biol. **49**(7), 1277–1294 (2004).
43. R. J. Zawadzki, C. Leisser, R. Leitgeb, M. Pircher, and A. F. Fercher, "Three-dimensional ophthalmic optical coherence tomography with a refraction correction algorithm," Proc. SPIE **5140**, 20–27 (2003).
44. V. Westphal, A. Rollins, S. Radhakrishnan, and J. Izatt, "Correction of geometric and refractive image distortions in optical coherence tomography applying Fermat's principle," Opt. Express **10**(9), 397–404 (2002).

1. Introduction

Measurements of changes in intraocular distances and crystalline lens shape with accommodation and with age are key factors to understanding the mechanism of accommodation and presbyopia; the loss of near vision with age. Measurements of the dynamic accommodative response are of particular interest in the development of models of the accommodative plant [1,2] and study of mechanics of accommodation [3]. In human eyes, other than changes in refraction [4–7], intraocular distances, including crystalline lens thickness, have been quantified dynamically [3,8–10]. Dynamic changes in the 2D shape of the anterior segment and crystalline lens can be imaged using Scheimpflug photography [11], but optical coherence tomography (OCT) is arguably the most promising modality for dynamic biometry of accommodation because of its 3 D imaging capability, high sensitivity, high resolution and high acquisition speed. Uhlhorn *et al.* [12] developed a time-domain OCT system (TD-OCT) with a long imaging depth of 10 mm in air for *in vitro* crystalline lens imaging. The low acquisition speed of TD-OCT does not make it suitable for *in vivo* dynamic studies. SD-OCT (Spectral-Domain) or SS-OCT (Swept-Source) offers the required speed but the challenge of these frequency domain methods is that they provide limited axial range if axial resolution is not to be compromised. There has been a growing interest in increasing the axial range of the current FD-OCT implementations to image and perform biometry of the anterior segment. Images of the whole anterior segment have been acquired at 830 nm with SD-OCT employing complex conjugate removal techniques to double the axial range [13,14], and at 1300 nm with SS-OCT without requiring complex conjugate removal methods [15]. The axial range of OCT needs to be further increased if full-length imaging and biometry of the human eye is required. Recently, SS-OCT using a novel MEMS-VCSEL light source [16] was demonstrated for *in vivo* very high speed imaging of the eye with an unprecedented imaging depth of 50 mm in air and no sensitivity loss. This new implementation could potentially produce full-length OCT images and biometry of the human eye. However, MEMS-VCSEL light sources for OCT are still in their developmental phase and not commercially available. A system that can utilize more readily available components may be of interest for many users.

Another challenge in imaging the full-length human eye is that the OCT delivery system needs to produce a large depth of focus to simultaneously obtain high signal strength from the anterior segment and the retinal structures while maintaining a sufficient transverse resolution. Simultaneous anterior segment and conventional retinal OCT imaging has recently been demonstrated using two separate SD-OCT systems [17], and an approach using one SS-OCT system with a novel dual beam delivery [18].

In this paper, we describe a method to perform ocular imaging and biometry of the full-length of the eye dynamically during accommodation by acquiring multiple OCT frames at a fast rate. An optical switch was implemented in the reference arm of an extended-depth SD-OCT system to enable imaging of multiple OCT frames at different depths without sacrificing axial resolution. The delivery probe of the OCT system was coupled with a custom-made module that provides accommodation and disaccommodation monocular step stimuli to allow imaging and measurement of the dynamic accommodative response of the eye from the anterior cornea to the retina.

#166403 - $15.00 USD Received 10 Apr 2012; revised 21 May 2012; accepted 1 Jun 2012; published 6 June 2012

2. Methods

2.1. SD-OCT system and performance

The SD-OCT system (Fig. 1) is a Michelson interferometer that consists of a 2 × 2 20/80 fiber coupler (FC850-40-20-APC, Thorlabs Inc, USA). The light source is a superluminescent diode (SLD) with a center wavelength of 840 nm and a FWHM (full width at half maximum) bandwidth of 50 nm (SLD-371-HP2, Superlumdiodes Ltd, Moscow, Russia). The configuration of the spectrometer in the detection arm is similar to the one reported by Grulkowski *et al.* [13]. The spectrometer consists of a collimating lens (HPUCO-23AF-830-S-60AC, OZ Optics, Canada), a 1800 line/mm transmission grating (HD1800, Wasatch Photonics, USA), an achromatic imaging lens (30.1395, f = 210 mm, Rolyn Optics, CA) and a line scan CMOS camera (Basler Sprint spL4096-104k; Basler AG, Germany) operating in summing mode between the two detector lines.

The calculated average spectral resolution of the spectrometer is 0.017 nm/pixel, which corresponds to a theoretical maximum ranging depth of about 10.63 mm in air [19]. An image acquisition board (PCIe-1429; National Instruments, USA) acquires the image captured by the

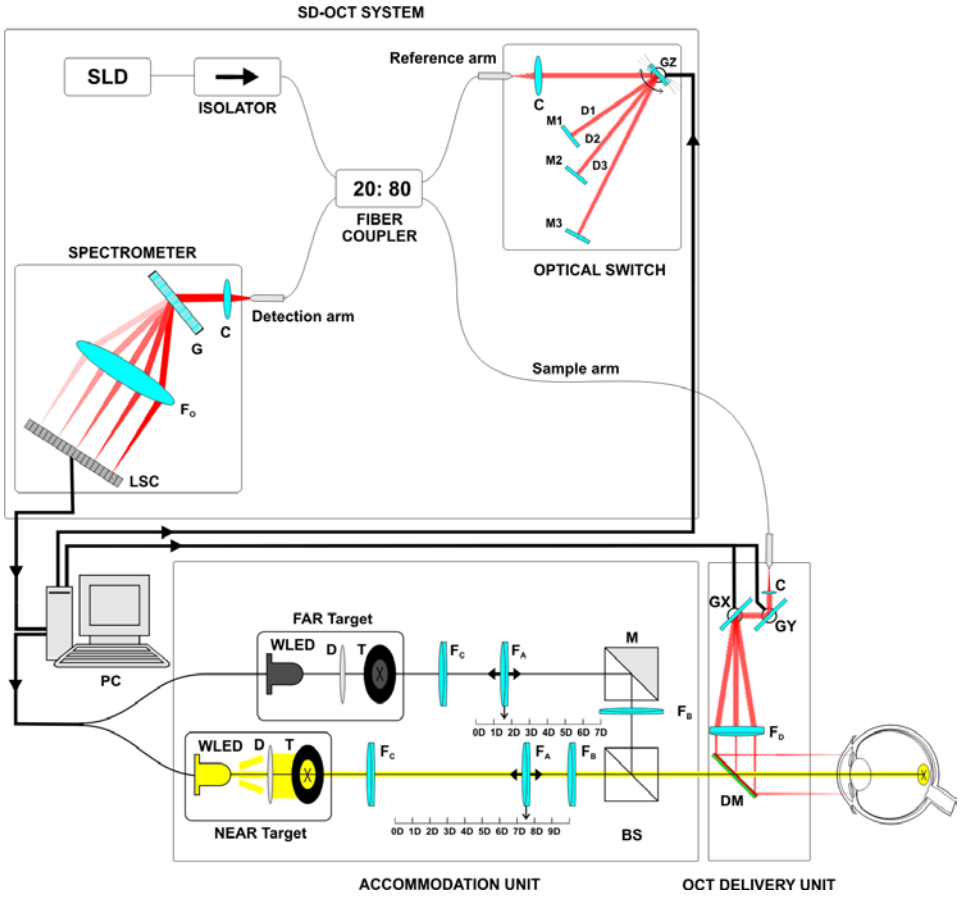

Fig. 1. Schematic of the accommodation OCT system. The SD-OCT system is shown with the Optical Switch in the reference arm. SLD: Light source. LSC: Line-scan camera. F_O: Objective lens of the spectrometer. C: Collimator. G: Grating. M1,M2,M3: Mirrors. GZ: Axial galvanometer scanner. The accommodation module and the OCT delivery unit are also shown. GX and GY: Transversal galvanometer scanners. F_D: Objective lens of the OCT delivery unit. DM: Dichroic mirror. BS: Beam splitter. M: 45° Mirror. F_B: Badal lens. F_A: Auxiliary lens. F_C: Collimating lens. T: Target. D: Diffuser. WLED: White light LED.

#166403 - $15.00 USD Received 10 Apr 2012; revised 21 May 2012; accepted 1 Jun 2012; published 6 June 2012

CMOS camera and transfers it to a computer workstation (Dell T5500, dual 3.6 GHz processor, 3 GB memory) for signal processing and real-time image display. A commercial software package was used for the real-time acquisition and display of the OCT data (Bioptigen, Inc. Research Triangle Park, NC).

The sensitivity fall-off and axial resolution of the SD-OCT system were characterized (Fig. 2) using published methods [20]. The sensitivity progressively decreases over the entire range from a peak of sensitivity of 98 dB at 100 μm from the zero-delay position to 55 dB at a depth of 10 mm, corresponding to a maximum sensitivity loss of about 43 dB. The measured axial range was 10.43 mm, which is in agreement with the theoretically predicted value (10.63 mm). At depths below 7 mm the FWHM of the PSFs was approximately equal to 8 μm. Beyond 7 mm the free-space axial resolution progressively degrades, until it reaches 14 μm at the end of the axial range. Reasons for the axial resolution decay with depth have been discussed by others [21,22].

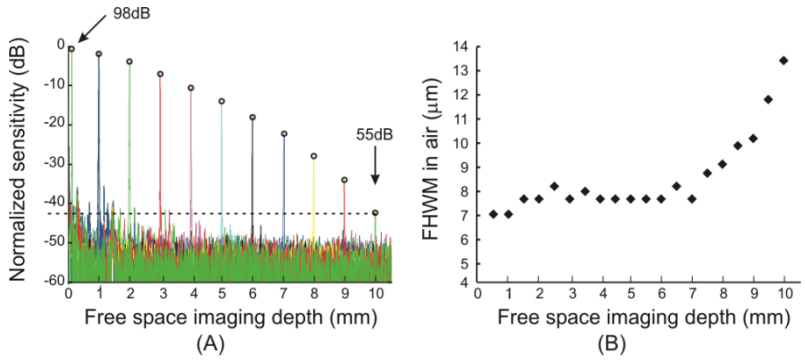

Fig. 2. Plot of the sensitivity as a function of depth (A) and FWHM of the axial point spread functions (B).

2.2. Reference arm optical switch

To extend the effective imaging depth an optical switching method similar to the one reported by Wang *et al.* [23] was implemented in the reference arm (Fig. 3A). The optical switch consists of an aspheric lens collimator C (C220TME-B f = 11 mm, Thorlabs, USA), a galvanometer optical scanner GZ (6210H, Cambridge Technology, Inc., USA) and three free-space optical delay lines (D1, D2, and D3) that are radially arranged around the axis of rotation of GZ. The optical delay lines D1, D2 and D3 use three mirrors M1, M2 and M3 (05D20ER.2, Newport, Inc., USA) as retro-reflectors. Each mirror is mounted on a precision linear stage (LS) with an actuator sensitivity of 1 μm (BM11.25, Newport, USA) that is used to set the optical delay introduced by each delay line. During image acquisition, the mirror mounted on the galvanometer scanner GZ sequentially deflects the reference beam to the three optical delay lines. The optical path difference between the three delay lines, d_{12} and d_{23} (Fig. 3(A)), determines the axial offset between the three frames (F1, F2 and F3). The axial offsets of the three frames are precisely calibrated so that the system allows imaging of the full-length anterior segment and the retina for an emmetropic adult eye (Fig. 3(B)). The control signal V_{GZ} of GZ is synchronized with each end of frame (EOF) acquisition event (Fig. 3(C)). The switching time of the custom-made optical switch includes the galvanometer settling time (~100 μs) and the time it takes the scanner to traverse the necessary angle. With the current configuration, the average switching time t_S between two consecutive delay lines is about 200 μs.

#166403 - $15.00 USD Received 10 Apr 2012; revised 21 May 2012; accepted 1 Jun 2012; published 6 June 2012

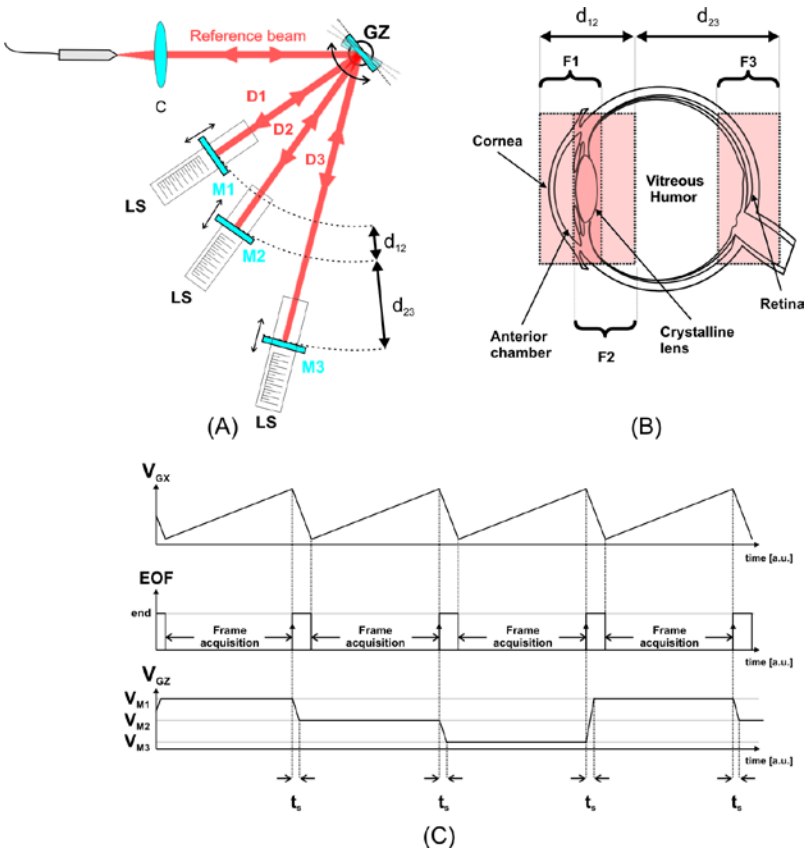

Fig. 3. (A) Schematic of the optical switch. GZ: axial galvanometer scanner. D1, D2 and D3: delay lines. M1, M2, and M3: mirrors. LS: linear stage. (B) Multiple frame acquisition. Frames F1 and F2 cover the anterior segment. Frame F3 covers the retina. (C) Timing diagram of the switching operations. During a frame acquisition, the signal V_{GZ} is constant so that the reference beam is maintained at a specific delay line. The reference beam is then commuted to the next delay line at the end of a frame acquisition and during the inactive operation of the transversal galvanometer mirrors G_X and/or G_Y. The optical switch operates during the inactive return scan of the lateral scanners. V_{GX}: control signal of the transversal horizontal galvanometer scanner. EOF: end of frame event. V_{GZ}: control signal of the axial horizontal scanner. t_S: average switching time t_S = 200 µs. V_{M1}, V_{M2} and V_{M3}: V_{GZ} values corresponding to the reference beam aligned along the delay lines D1, D2 and D3, respectively. d_{12} and d_{13} are the optical paths differences between the delay lines.

2.3. Sample arm

The OCT sample arm consists of an aspheric lens collimator (C220TME-B, f = 11 mm, Thorlabs, USA), an X-Y galvanometer optical scanner (6210H, Cambridge Technology, Inc., USA) and an NIR achromatic objective lens (AC254-100-B, f = 100 mm, Thorlabs, USA). The collimator produces a 1.8 mm diameter beam. The objective lens is aligned to provide a telecentric scan with flat field along the horizontal axis (X). In this study the vertical scanner (Y) was not used. The focused beam has a diameter of 52 µm at the waist and a depth of focus (two times the Rayleigh range) of 5.1 mm in air. During imaging, the focal plane of the scanning beam is positioned slightly posterior to the mid-point of the crystalline lens. Under these conditions, we estimated the beam diameter of the diffracted limited spot at the cornea and retina positions by computer simulation (ZEMAX) using Gullstrand's schematic eye. The approximate beam diameter is about 100 µm at the cornea and about 300 µm at the retina. The power delivered to the eye is 750 µW [24].

#166403 - $15.00 USD Received 10 Apr 2012; revised 21 May 2012; accepted 1 Jun 2012; published 6 June 2012

2.4. Accommodation module

Two accommodation modules based on a variation of the Badal optometer [25,26] were built to provide monocular accommodation step stimuli (Fig. 1). The two modules are optically coupled to ensure mutual alignment, thereby eliminating target parallax 'jump' during accommodation/disaccommodation. One module provides a low vergence stimulus (FAR target) while the other provides a high vergence stimulus (NEAR target). Each module consists, in sequence, of a high contrast cross target placed at the focal point of a +13.3 D collimating lens (F_C), an auxiliary +6.7 D lens (F_A) and a +13.3 D Badal lens (F_B). The position of F_A along its optical axis is adjusted by the operator to set the amplitude of the step stimulus from 0 to 9.5 D. The targets of each Badal module are retro-illuminated using the diffuse light produced by a light emitting diode (WLED). The targets are visible to the subjects only when they are illuminated. A step stimulus is thus provided to the subject by alternately illuminating the two targets. The step direction for an accommodation stimulus (far-to-near) is set by first illuminating the FAR target. The opposite sequence provides a disaccommodation step stimulus. The step stimulus is synchronized with the acquisition of the OCT. The accommodation module was coupled with the OCT delivery system using a dichroic mirror, DM (NT64-470, Edmund Optics, NJ). The integrated OCT delivery system and accommodation module was mounted on a table equipped with a joystick and head-rest.

3. Results

3.1. Extended imaging of the eye

The imaging system can operate in three different modes, corresponding to the number of delay lines used. The imaging system was first tested using only delay line D2 (Fig. 4). A 35 year-old subject was instructed to fixate on the distance target set at 0 D (accommodation relaxed), and an image was acquired along the horizontal meridian of the eye. The system was adjusted so that the zero-delay position, which produces the highest sensitivity, corresponds to the posterior lens (bottom of the image in Fig. 4). The apex of the cornea is not visible in the image because of the limited axial range. The effect of the sensitivity fall-off with depth is also observable. The signal strength at the cornea, which is located at the end of the depth range, is significantly lower.

Images of the full anterior segment with higher sensitivity were acquired on the same subject with accommodation relaxed by switching between delay lines D1 and D2 to acquire two images at different depths (F1 and F2 in Figs. 5(A) and (B)). The optical path difference

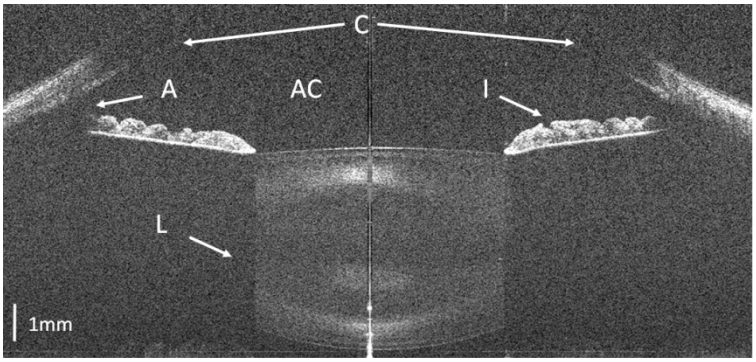

Fig. 4. Single frame OCT image of the anterior segment of a 35 year-old human eye. The main ocular structures are indicated: cornea (C), anterior chamber (AC), crystalline lens (L), iris (I) and angle (A). The image consists of 1000 A-lines of 2048 pixels each. The size of the frame in the axial direction is 7.6 mm when the mean group refractive index of the anterior segment is taken to be 1.37 at 840 nm. The lateral scanning length was set to 16mm. Zero-delay location (ZD) is indicated.

#166403 - $15.00 USD Received 10 Apr 2012; revised 21 May 2012; accepted 1 Jun 2012; published 6 June 2012

d_{12} was set to 13 mm. Frame F1 was acquired with the sensitivity peak (ZD1) located near the outer cornea (Fig. 5(A)) and frame F2 with the sensitivity peak (ZD2) located near the posterior lens (Fig. 5(B)). After acquisition, the regions of low sensitivity at depths longer than $d_{12}/2$ = 6.5 mm were removed from each frame (Figs. 5(C) and (D)). The cropped frames were then stitched to form a composite image (F1 + F2 in Fig. 5(E)). The composite frame consists of 500 A-lines and was acquired in about 50 ms. The axial number of pixels that were combined to compose the frame is 2556. The sensitivity drop at the center of the combined frame is about 18 dB (Fig. 5(E)). The resultant composite image of the anterior segment shows high signal strength from the cornea to the posterior lens.

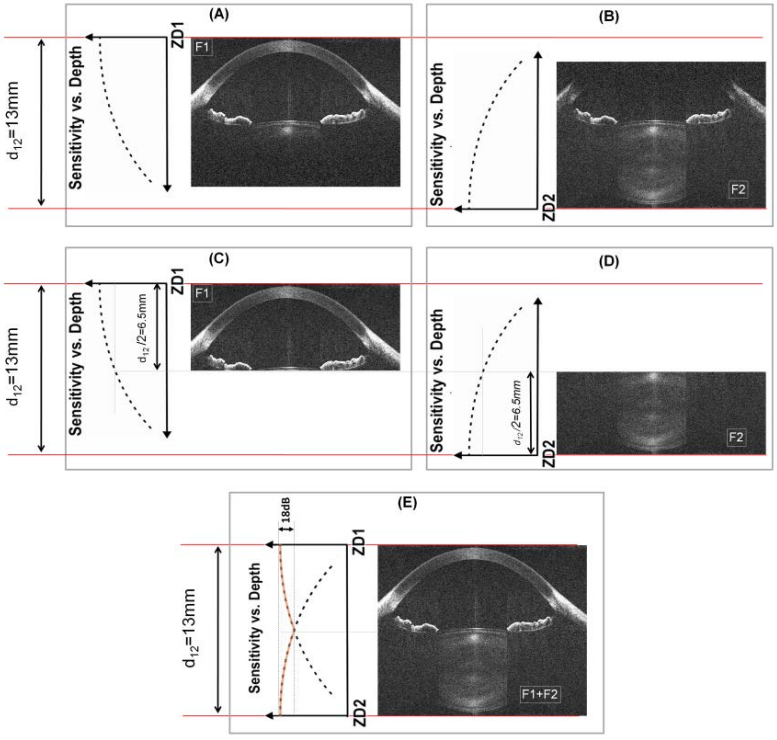

Fig. 5. Generation of an image of the full depth anterior segment of a 35 year-old subject using the optical switch with two delay lines (D1 and D2). (A) Image of the anterior segment (F1) with delay line D1. (B) Image of the anterior segment (F2) with delay line D2. Regions of low contrast were removed from frame F1 (C) and F2 (D) at depths longer than $d_{12}/2$ = 6.5 mm. (E) Cropped frames F1 and F2 are joined. The composite frame consists of 500 (lateral) × 2556 (axial) pixels. The size of the composite frame in the axial direction is 13 mm when the mean group refractive index of the anterior segment is taken to be 1.37 at 840 nm. The lateral scanning length was set to 16mm.

Images of the anterior segment and retina were acquired in the same 35 year old subject with accommodation relaxed by switching between D1, D2 and D3 (Fig. 6). The anterior segment was imaged with the same parameters as before. The free-space optical path difference between the delay lines D2 and D3 was set to d_{23} = 24 mm so that for an emmetropic eye the zero-delay position (ZD3) is near to the vitreo-retinal boundary. Frame F3 consists of 500 A-lines each of 2048 pixels. The composited image resulting from the combination of the three frames F1, F2 and F3 was acquired in about 75 ms. No effort was made to image the vitreous chamber length because there are no structures of interest to our studies in this region. In principle, it is possible to image the vitreous by adjusting the zero-delay position of delay line D3 or adding additional delay lines to image the entire length of the eye.

#166403 - $15.00 USD Received 10 Apr 2012; revised 21 May 2012; accepted 1 Jun 2012; published 6 June 2012

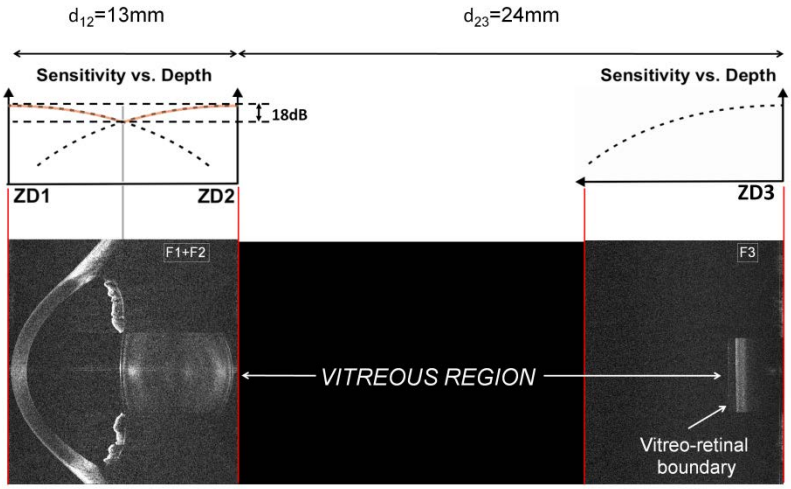

Fig. 6. Generation of an image of the full-length anterior segment and the retina of a 35 year-old subject using the optical switch with three delay lines (D1, D2 and D3). The composite OCT image of the anterior segment (F1 + F2) together with the retina (F3) consists of 500 A-lines × 4604 (axial) pixels. Most of the vitreous chamber length is not imaged.

3.2. Imaging and biometry of static accommodation

The optical switch was set to sequentially commute between the two delay lines D1 and D2 to acquire full-depth images of the anterior segment in the right eye of a 24 year-old and the same 35 year-old subjects at 0 D and 7 D target vergence (Fig. 7). Changes in curvature and thickness of the crystalline lens are observed in the 24 year-old subject. As expected, the lens is thicker and its surfaces are steeper in curvature in the accommodated state (7 D stimulus) compared to the relaxed state (0 D stimulus).

For the 35 year-old subject, the changes in lens shape are significantly reduced, a consequence of the loss of accommodation with age. The unaccommodated lens of the 35 year-old subject (Fig. 7(C)) is also thicker than that of the 24 year-old lens (Fig. 7(A)), due to

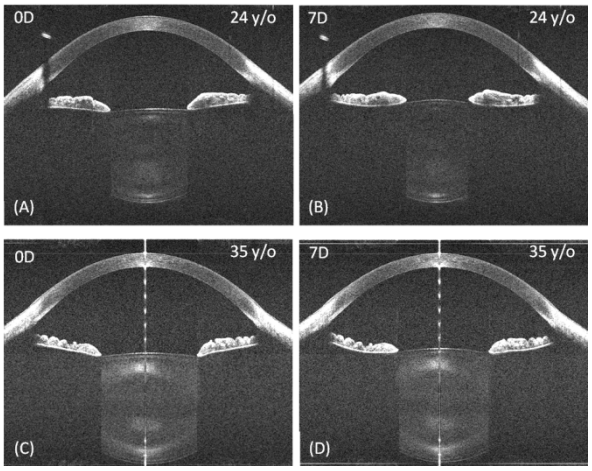

Fig. 7. OCT cross-sectional images of the lens acquired: on a 24 year-old subject in the relaxed state (A) and in response to a 7 D accommodative stimulus (B), and on a 35 year-old subject in the relaxed state (C) and in response to a 7 D accommodative stimulus (D). Image density: 1000 A-lines × 2556 (axial) pixels. The size of the composite frame in the axial direction is 13 mm when the mean group refractive index of the anterior segment is taken to be 1.37 at 840 nm. The lateral scanning length was set to 16mm.

#166403 - $15.00 USD Received 10 Apr 2012; revised 21 May 2012; accepted 1 Jun 2012; published 6 June 2012

the continuous growth of the lens even in adulthood. The OCT images also show that pupil constriction during accommodation is different in the two subjects with the older subject exhibiting less change on accommodation. In addition, the backscattered signal strength is stronger in the 35 year-old lens due to the progressive age-related changes in lens scattering [27].

3.3. Imaging and biometry of dynamic accommodation

The accommodative response to a step stimulus from 0 D to 7 D was imaged dynamically in the right eye of the same subjects. A total of 50 composite cross-sectional images of the full-length anterior segment, each consisting of two frames, were continuously acquired at a frame-rate of 12.5 frames per second, for a total duration of 4 s. Each OCT image consisted of 500 A-lines. Images were acquired along the horizontal meridian (Fig. 8).

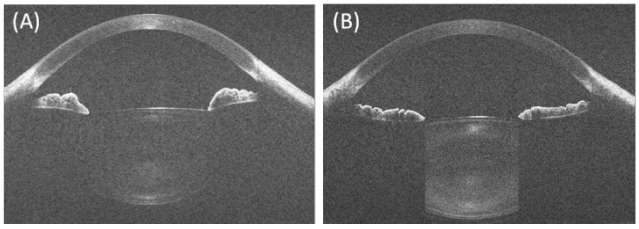

Fig. 8. Real-time display of lens accommodation in a 24 year-old subject (Media 1) (A) and a 35 year-old subject (Media 2) (B). The movies were recorded during the accommodative responses from relaxed state (0 D stimulus) to a 7 D stimulus. The OCT images in the movies are continuously displayed at 12.5 fps during the accommodative responses from the relaxed state (0 D stimulus) to a 7 D accommodative stimulus.

Full-length ocular biometry was performed on the 35 year-old subject during accommodation and disaccommodation (Fig. 9). First, the accommodation module was set to provide a step stimulus from 0 D to 4 D (accommodation).The far stimulus (0 D) was illuminated and the subject was instructed to fixate the target.

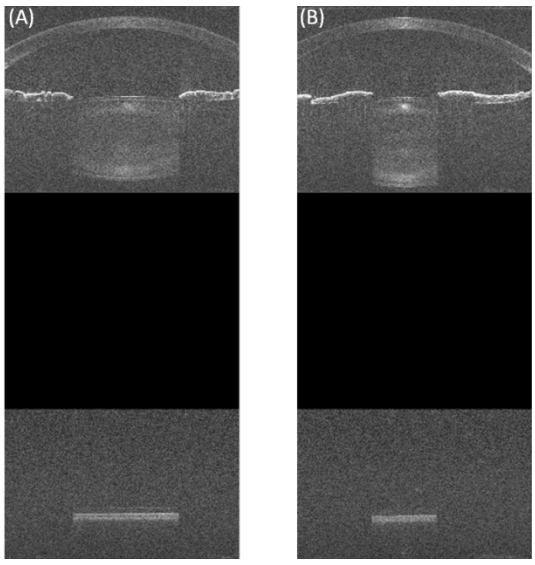

Fig. 9. (A) Real-time full-length display of accommodation in a 35 year old subject in response to a step stimulus from 0 D to 4 D (Media 3). (B) Real-time display of disaccommodation in response to a step stimulus from 4 D to 0 D (Media 4). The frame rate of the composite OCT images of the anterior segment and the retina in the movies is 8.25fps.

#166403 - $15.00 USD Received 10 Apr 2012; revised 21 May 2012; accepted 1 Jun 2012; published 6 June 2012

A total of 33 composite frames of the anterior segment and the retina were acquired during the accommodation response along the horizontal meridian. The same experiment was repeated with the accommodation module set to provide a step stimulus from 4 D to 0 D (disaccommodation). Each OCT image consists of 500 × 4604 pixels (lateral × axial). The lateral scanning width was set to 10 mm. Intraocular optical distances including corneal and crystalline lens thicknesses, anterior chamber depth and the distance from the outer cornea to retinal pigment epithelium boundary were measured along the central axis on the OCT composite frames acquired during accommodation and disaccommodation.

To quantify the intraocular distances the ocular surfaces were first segmented in the OCT images over a central region of the eye with lateral width of about 1mm. The optical distances between the segmented ocular surfaces were then calculated along the central axis. The geometrical lengths were obtained by dividing the measured optical path lengths by the group refractive index of the ocular media at 840 nm [12,28–30] (Table 1). The axial length of the eye was calculated as the sum of cornea, aqueous, lens, vitreous and the retina geometrical lengths.

Table 1. Group refractive index of the cornea [28], the crystalline lens [12] and the aqueous, vitreous humors [29] and retina [30] at 840 nm used to convert optical distances

Ocular tissue	Refractive index (at 840 nm)
Cornea	$n_C = 1.387$
Aqueous humor	$n_A = 1.342$
Crystalline lens	$n_L = 1.415$
Vitreous	$n_V = 1.341$
Retina	$n_R = 1.380$

Figure 10 shows the dynamics of the ocular length changes. The dynamic measurements show minor fluctuations, but no overall trend, in eye length (Figs. 10(E) and (F)) and corneal thickness (Figs. 10(G) and (H)) during the dynamic responses. Mean and standard deviation of the axial length of the eye and the corneal thickness were calculated before and after the stimulus onset (Table 2). The differences in mean corneal thickness across different accommodative states are comparable to the axial resolution of the system and are attributable to the measurements uncertainty. The mean eye axial length across the accommodative states shows larger variations compared to the corneal thickness measurements. The larger uncertainty affecting the eye axial length is possibly attributable to motion artifacts due to eye movements occurring during the acquisition of the three consecutive frames. The crystalline lens thickness increases during accommodation (Fig. 10(G) red line) and decreases during disaccommodation (Fig. 10(H) red line), as expected.

Table 2. Mean and standard deviation of the corneal thickness, eye axial length, anterior chamber depth and crystalline lens thickness during accommodation and disaccommodation in a 35 year old subject

	Accommodation		Disaccommodation	
Ocular axial distances	0 D	4 D	4 D	0 D
Cornea thickness (mm)	0.556 ± 0.004^a	0.560 ± 0.003^b	0.556 ± 0.002^a	0.554 ± 0.003^b
Eye axial length (mm)	24.93 ± 0.025^a	24.93 ± 0.019^b	24.97 ± 0.012^a	24.98 ± 0.017^b
Anterior chamber depth (mm)	3.49 ± 0.015^a	3.42 ± 0.020^c	3.45 ± 0.034^a	3.53 ± 0.012^c
Crystalline lens thickness (mm)	4.02 ± 0.004^a	4.23 ± 0.008^c	4.32 ± 0.005^a	4.07 ± 0.008^c

[a]Mean and standard deviation of the intraocular distances were calculated on 12 samples acquired before the stimulus onset ($t < 1.45$ s).
[b]Mean and standard deviation of the intraocular distances were calculated on 21 samples acquired after the stimulus onset ($t > 1.45$ s).
[c]Mean and standard deviation of the intraocular distances were calculated on 5 samples acquired at the end of the acquisition process ($3.4 \text{ s} < t < 4$ s).

#166403 - $15.00 USD Received 10 Apr 2012; revised 21 May 2012; accepted 1 Jun 2012; published 6 June 2012

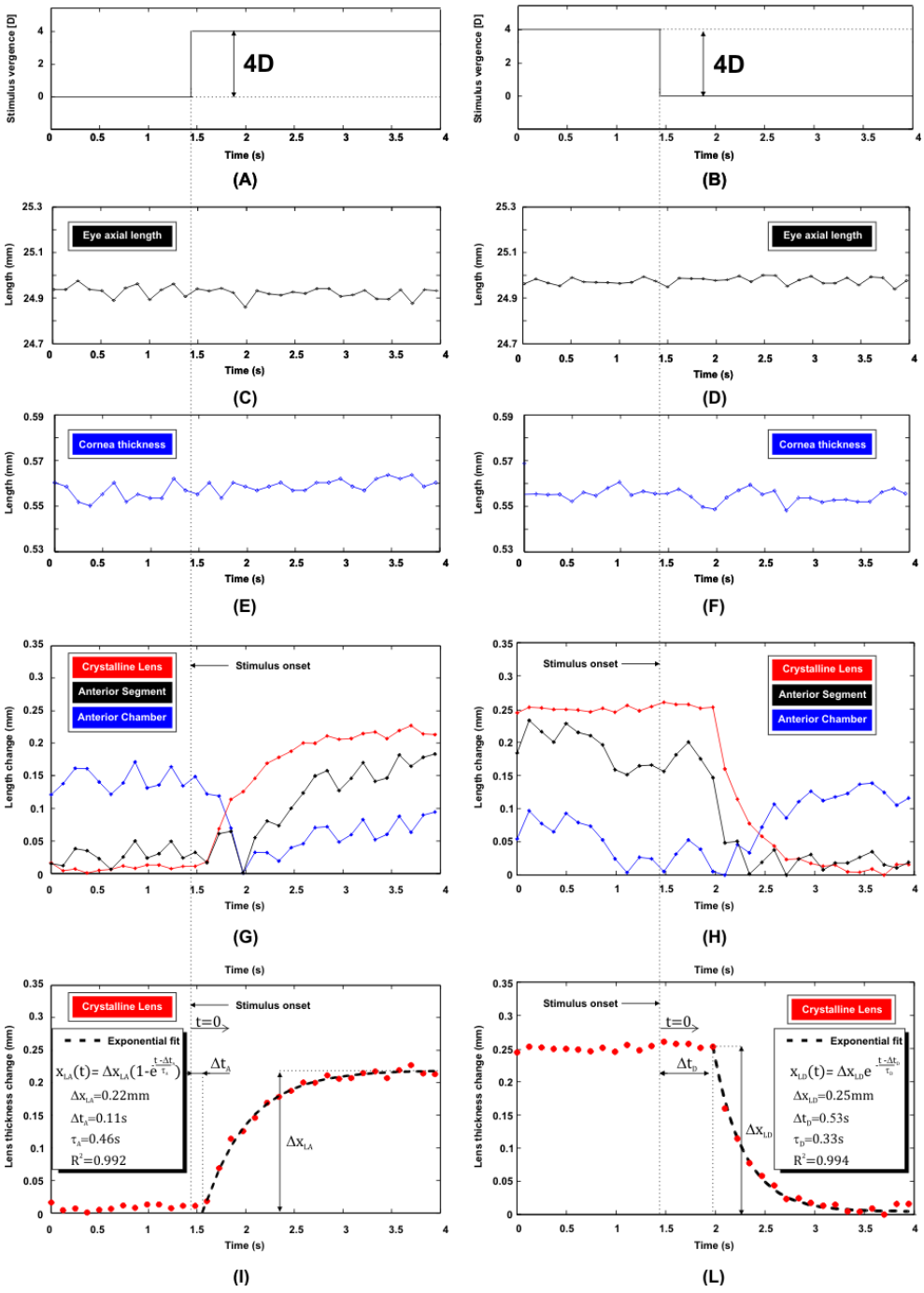

Fig. 10. (A) Step stimulus from 0 D to 4 D. (B) Step stimulus from 4 D to 0 D. (C and D) Dynamics of the axial eye length in response to the accommodation stimulus (C) and the disaccommodation stimulus (C). (E and F) Dynamics of the axial eye length in response to the accommodation stimulus (E) and the disaccommodation stimulus (F). (G and H) Dynamics of the ocular distance changes in response to the accommodation stimulus (G) and the disaccommodation stimulus (H). The displayed length changes were calculated by subtracting from the measurements the minimum value measured in the relaxed state. (I and L) Exponential fits of the time dependent change in lens thickness during accommodation (I) and disaccommodation (L).

#166403 - $15.00 USD Received 10 Apr 2012; revised 21 May 2012; accepted 1 Jun 2012; published 6 June 2012

The mean absolute thickness changes in the crystalline lens are 0.22 mm and 0.25 mm during accommodation and disaccommodation, respectively (Table 2). These values are comparable with the range of measurements published by Dubbelman *et al.* [31], which found a mean change in lens thickness (±s.d.) of 0.18 (±0.048) mm for a 4D stimulus. The anterior chamber depth decreases during accommodation (Fig. 10(G), dark blue line) while it increases during disaccommodation (Fig. 10(H), dark blue line). The mean absolute changes in anterior chamber depth are 0.07 mm and 0.08 mm during accommodation and disaccommodation, respectively (Table 2). These values are within the measurement variability of the anterior chamber depth changes found by Dubbelman *et al.* [31] for a 35 year old subject and a 4D stimulus, which approximately ranges from 0.06 to 0.22 mm. The dynamics of the anterior segment length, which is measured as the distance from the anterior cornea to the posterior lens, are a result of the combination of the changes in the thickness and the axial shift of the lens during accommodation and disaccommodation. Figure 10(G) (black line) shows that the anterior segment length increases during accommodation and decreases during disaccommodation (Fig. 10(H)- black line). The step response results of the crystalline lens thickness to a target vergence demand (Figs. 10(G) and (H), red lines) are similar to those obtained using continuous high-resolution A-scan ultrasonography [3]. We fit the time-dependence of the lens thickness with the following exponential growth and decay functions for, respectively, accommodation (Fig. 10(I)) and disaccommodation (Fig. 10(L)) [3]:

$$x_L(t) = \Delta x_L \left(1 - e^{-\frac{t-\Delta t}{\tau}}\right) \quad (1)$$

$$x_L(t) = \Delta x_L e^{-\frac{t-\Delta t}{\tau}} \quad (2)$$

where t is time elapsed from the step stimulus onset, $x_L(t)$ is the time dependent crystalline lens thickness, Δx_L is the total lens thickness change, Δt is the latency time, which is the time elapsed between the application of the step stimulus and the start of the accommodation response; τ is the time constant of the response. During accommodation and disaccommodation the estimated latency times from fitting to measurements are Δt_A = 0.11 s and Δt_D = 0.53 s, respectively. The time constants of accommodation and disaccommodation were, respectively, τ_A = 0.46 s and τ_D = 0.33 s, which are comparable with the ones calculated using ultrasonographic biometry [3]. The absolute lens thickness changes during accommodation and disaccommodation are, respectively, Δx_{LA} = 0.22 mm and Δx_{LD} = 0.25 mm. The velocity of the time dependent change in lens thickness was calculated by taking the first derivative of the fit in Eq. (1) and (2) for accommodation and disaccommodation, respectively. During accommodation the peak velocity is equal to $\Delta x_{LA}/\tau_A$ = 0.48 mm/s. During disaccommodation the peak velocity is equal to $-\Delta x_{LD}/\tau_D$ = –0.76 mm/s.

4. Discussion

In this study, we used a SD-OCT system that produces a free-space axial range of 10.43 mm in air. The system is affected by significant sensitivity decay with depth. Furthermore, the images of the anterior segment produced by the OCT engine alone are barely sufficient to display the full thickness of the anterior segment of young subjects. In addition, even in younger subjects, the sensitivity fall-off reduces the contrast of the regions of the image that are distant from the zero-delay position. Three frames were used to image the full-length of the eye by using an optical switch technique implemented in the reference arm of the OCT system. The optical switch sequentially commutes the reference beam to three delay lines with different optical path lengths allowing shifts of the axial location of the OCT frame acquisition. The anterior segment was imaged entirely with high contrast along its depth by combining two overlapping frames. The retina was imaged in a third separate frame distant in

#166403 - $15.00 USD Received 10 Apr 2012; revised 21 May 2012; accepted 1 Jun 2012; published 6 June 2012

depth from the first two. The abrupt deterioration of the sensitivity fall-off associated with the SD-OCT system used in this study limits the axial range generated by combining the two overlapping frames to about 13 mm, which is sufficient to image the anterior segment along its full depth.

The main advantage of using an optical switch [23] is that the method can be used to extend the imaging axial range of any Fourier Domain OCT implementation without sacrificing axial resolution. Hence, any improvement to the sensitivity roll-off and/or axial range of the OCT system used in combination with the optical switch will extend the imaging range produced by the combination of two or more frames. The main drawback is that a trade-off exists between the number of frames sequentially acquired and the frame rate [23]. In our implementation, for instance, the frame rate is reduced by a factor of three with respect to the original imaging rate produced by the SD-OCT system. The use of a fiber-optic switch has been proposed by Wang *et al.* [23] to increase the imaging range of an SD-OCT system. One advantage of using a free-space switch is that it does not introduce optical dispersion across channels, which is typical of fiber-coupled optical switches. Another advantage of using a free-space switch is that the switching time (200 μs) is shorter compared to the typical switching time of a commercial fiber-coupled optical switch operating in the wavelengths region around 800 nm. The switching time, which is two orders of magnitude less than the acquisition time of a single frame (25-40 ms), is not a limiting factor for the frame rate. Since the current custom-made switch produces high commutation rates, it can be used in combination with high speed state of the art FD-OCT systems if higher frame rate is needed. In addition, the current switching time can be further reduced by optimizing the optical configuration of the switch as, for example, by reducing the angular displacement between the delay lines and/or using galvanometer scanners with higher speed.

Dynamic focusing [32–35] and multiple-focus beam [36,37] methods have been proposed in OCT systems to maintain high lateral resolution over the whole depth scan. These approaches often use moving parts and/or more intensive image processing, which in turn increase the system complexity and lower the imaging speed. The results of this study demonstrate that one-dimensional biometry of the whole eye can be performed with OCT without the need of dynamic focusing nor a multiple-focus beam. A drawback of using a static single-focus beam approach is that the lateral resolution performance is sacrificed to lower the system complexity. The delivery optics were designed to produce a focused spot with a diameter of about 52 μm and a long depth of focus of 5.1 mm. The beam waist was positioned slightly posterior to the mid-point of the crystalline lens to obtain images of the anterior segment with high resolution. The beam diameter becomes substantially larger deeper in the eye (~300μm), which decreases the transversal resolution of the retinal image. Due to the refraction of the OCT beam at the cornea and lens surfaces, the image of the retina obtained with the current scanning configuration represents a narrow transversal region of the retina. As a result, the OCT image of the retina does not provide high resolution or wide-field structural information. However, the high signal strength produced by the retina enables quasi-simultaneous biometry of the anterior segment and measurements of the eye length, without requiring separate devices or a separate measurement. Among other applications, the ability to measure the axial eye length will enable us to back-calculate the power [38], or the equivalent [39] or average [12,40] refractive index of the crystalline lens.

In principle, the high-resolution and high-speed cross-sectional and volumetric imaging capabilities of SD-OCT and its quantitative nature should allow precise 2-D and 3-D measurements of the changes in lens structure during accommodation. One of the major impediments in doing so is image distortion due to the refraction of the probe beam at the interface between ocular surfaces. Image distortions due to refraction must be corrected, preferably in three-dimensions, in order to obtain valid biometric data such as intraocular distances, surface curvature and asphericity [41–44]. A distortion correction algorithm must

#166403 - $15.00 USD Received 10 Apr 2012; revised 21 May 2012; accepted 1 Jun 2012; published 6 June 2012

be implemented before we can obtain accurate quantitative two-dimensional biometry of the ocular surfaces during accommodation.

While stimulating and imaging accommodation, ocular convergence and movements may lead to errors in dynamic measurements of the intraocular distances. The cross-sectional nature of OCT provides a mean to assess if correct ocular alignment is maintained during the accommodation response. The movies of the accommodation process (Fig. 8 and 9) suggest that convergence of the eye is minimal during imaging. Similar results were found by dynamically imaging accommodation along a meridional-vertical plane. The monocular accommodation module was designed specifically to reduce changes in alignment of the test-eye between accommodated and disaccommodated states. However, the image acquisition time is not short enough to completely eliminate the effect of eye movements during the acquisition of a composite frame. Assuming the axial length of the eye is constant during accommodation, the variability of the eye axial length (Table 2) provides an estimate of the impact of motion artifacts on the measurement accuracy. In our measurements (Table 2), the axial length variability is relatively small (~0.02mm), which indicates that intraocular distance measurements performed with our setup are not severely deteriorated by motion-related artifacts. The detrimental effect of motion artifacts may be more critical if changes of shape of the eye components (e.g. radius of curvature of the ocular surfaces) need to be measured dynamically. In static ocular imaging, the acquisition speed is generally increased to reduce the total recording time and minimize the effect of motion-related artifacts. Increasing the imaging speed of our system would reduce the motion artifacts occurring during the acquisition of a composite frame. It would also allow acquisition of 3D-OCT data sets of the accommodation dynamics, which in turn would allow precise image registration and therefore correct for eye movements.

5. Summary

We have demonstrated that a SD-OCT system together with an optical switch implemented in the reference arm is capable of imaging the full length anterior segment and the retina. An accommodation target that provides monocular accommodation and disaccommodation step stimuli was developed and combined with the OCT delivery probe. The high speed of the system enables imaging of the dynamic process of accommodation. Intraocular distances were quantified dynamically along the central axis of the eye. The results show that OCT with single focus can image the eye and measure the dynamic changes of the intraocular distances during accommodation.

Acknowledgments

The study was supported in part by National Eye Institute Grants 2R01EY14225, F32EY15630 (Ruth L. Kirschstein National Research Service Award, Uhlhorn), P30EY14801 (Center Grant); the Florida Lions Eye Bank; the Henri and Flore Lesieur Foundation (J. M. P); an unrestricted grant from Research to Prevent Blindness; and the Australian Federal Government Cooperative Research Centre Scheme through the Vision Cooperative Research Centre.

#166403 - $15.00 USD Received 10 Apr 2012; revised 21 May 2012; accepted 1 Jun 2012; published 6 June 2012